Novel Detectors for Fluorescence Lifetime Imaging on the Picosecond Time Scale

Klaus Kemnitz,[1,4] Lutz Pfeifer,[2] René Paul,[2] and Maïté Coppey-Moisan[3]

Simultaneous acquisition of time and space information on the picosecond time scale became feasible with a recent advance in microchannel-plate photomultiplier-tube (MCP-PMT) technology: we present two novel MCP-PMT detectors for time- and space-correlated single-photon counting (TSCSPC), featuring a space-sensitive delay-line (DL) anode and quadrant anode (QA), respectively. The linear DL-MCP-PMT is characterized by a spatial instrument response function (IRF) of 100-μm FWHM, resulting in 200 space channels, whereas the QA-MCP-PMT is a 2D imager with 400 × 400 pixels at 40-μm resolution. The detectors have a temporal IRF of 75 ps (DL) and 80 ps (QA) FWHM, sufficient for 10 ps time resolution, at a dynamic range of 10^5 of the uncooled detector. A throughput of 10^5 cps is possible; in the imaging mode without timing, the QA-detector can achieve 10^6 cps. We present time-resolved spectroscopy of DNA probes (DAPI, TOTO, C350) in solution, in micelles, complexed to DNA, protein, and fixed cells. Aging of DAPI stock solutions is reported. A polarity model for the photophysics of DAPI is proposed. First microscope lifetime images on the picosecond time scale show a clear potential for dynamic stray-light rejection and kinetic discrimination of probe–protein and probe–DNA complexes.

INTRODUCTION

Simultaneous TSCSPC spectroscopy, based on novel MCP-PMTs, was introduced recently.[1] By replacing the disk anode of a standard MCP-PMT with a DL or quadrant anode, we gain access to space information along *x*- and *xy*-directions, respectively. TSCSPC is a variant of TCSPC,[2] a well-established method for the acquisition of fluorescence dynamics on the picosecond time scale of very weakly emitting sources that is distinguished by its unsurpassed dynamic range. IRFs as narrow as 16 ps can be achieved in single-channel 6 μm MCP detectors, resulting in an effective time resolution

of about 2 ps after deconvolution and indicating the ultimate time resolution of this technology.

EXPERIMENTAL

TSCSPC Spectroscopy Systems

Standard MCP-PMT and the novel DL and QA detectors are of identical construction, with the exception of the anode, as shown in Fig. 1. The determination of the *x*-space coordinate in the DL system is based on a measurement of travel time difference;[3] the *xy*-space in the QA system, in contrast, by measuring charges. In both detectors the incident photon produces a cone-shaped cloud of electrons at the output face of the second MCP that hits the DL or quadrant anode at a spatial position identical to that of the photon. The electric pulse

[1] EuroPhoton GmbH, Mozartstr. 27, D-12247 Berlin, Germany.
[2] LaserLabor Adlershof e.V., Rudower Chaussee 6, D-12484 Berlin, Germany.
[3] Institut Curie, 26 Rue d'Ulm, 75231 Paris, Cedex 05, France.
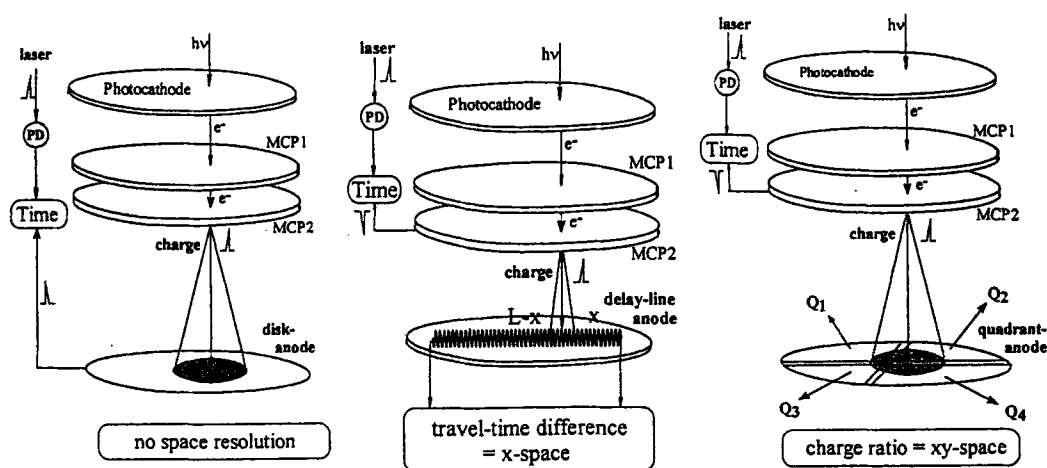[4] To whom correspondence should be addressed.

Fig. 1. Comparison of ELDY's DL and QA detectors with standard MCP-PMT.

is split into two or four portions, by the DL or quadrant anode, respectively. The two pulses of the DL system are amplified, discriminated, and used as the start and stop pulse in a time-to-amplitude converter (TAC), with the travel-time difference indicating the x-position. In the case of the QA system, the collected charges at the four segments are amplified by charge-sensitive, shaping amplifiers and read out by analog–digital circuitry and software.[4,5]

There are two ways to gain the time information: (a) a 2D multichannel analyzer (MCA), equipped with transputer and local memory, calculates time and space coordinates from the sum and difference, respectively, of both TAC outputs in a convoluted scheme (DL);[1] and (b) both TACs are independent and sum/difference calculation is not necessary,[1] and the timing information is derived from an auxiliary pulse, drawn from the second MCP, that is inverted, amplified, discriminated, and then fed as a start pulse into a TAC, together with a stop pulse from a photodiode as in standard TCSPC (DL and QA; Fig. 1). The best field data so far for the QA-system are FWHM(t) = 80 ps, 400 × 400 space channels, and 10^5 cps throughput. The present system has a resolution of FWHM(xy) = 40 μm within the central 16 mm of the total useful area of 24-mm diameter.[6] In the imaging mode without time resolution, 10^6 cps can be obtained.

The standard 12 μm MCP-PMT detector (Fig. 1, left) can achieve an IRF of FWHM = 36 ps, indicating the domain that might eventually be reached by DL and QA systems.

Materials and Methods

POPOP, PPO, SDS, and spectrograde solvents were from Aldrich, DAPI and TOTO from Molecular Probes,

C350 from Lambda, DNA (herring sperm) from Sigma, λ-DNA from Eurobio, and albumin from Bovine Serum. Monkey kidney cells were grown as monolayers and fixed at room temperature.

Second (385 nm) and third (257 nm) harmonics of a Ti–Saph laser (Lexel) with a pulse width of 1 ps were used for UV excitation (IRF FWHM = 75 ps) and an argon ion laser of 150 ps pulse width for excitation in the green at 514 nm (IRFWWHM = 300 ps). The time window in most measurements was 10 ns at a time resolution of 10 ps/channel.

Two DL systems were employed: one for spectroscopy, equipped with a polychromator (370-nm bandpass), and one for microscopy, utilizing a modified Leitz Orthoplan fluorescence microscope. Software for kinetic global analysis was from Globals Unlimited.

RESULTS

Reference Systems

Figure 2 shows three kinetic reference systems, used to characterize the performance of the DL detector in Fig. 1. The contour map and global analysis of PO-POP is shown at the top left. We obtain τ = 1.06 ± 0.02 ns, in agreement with the literature.[7] The retrieved lifetimes of the individual space channels are within the global error across the sensitive area of the detector; slight deviations at the fringes are due to small background contributions that influence the lifetime at weak signal strengths. The binary reference system PO-POP/PPO is shown at the bottom left, demonstrating a lifetime separability of 20%, i.e., 1.1 and 1.3 ns. Recov-
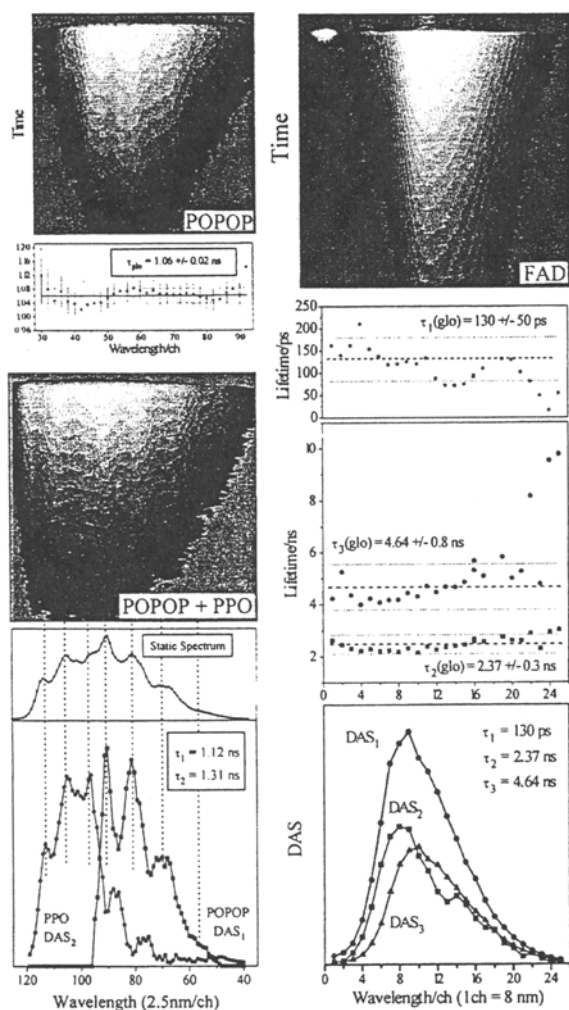
Fig. 2. Reference systems. Top left: Contour map and global analysis of POPOP/cyclohexane (undegassed), $c_0 = 3 \times 10^{-6}$ M, ex = 375 nm, 1 ch(x) = 2.5 nm, 1 ch(t) = 10 ps. Time axis (5 ns), top to bottom. Right: Contour map and three-exponential global analysis of 1×10^{-5} M FAD in water with decay-associated spectra (DAS). Bottom left: Contour map (top), integrated emission spectrum (center), and 80-channel global analysis with DAS of the binary reference system 3×10^{-6} M POPOP/PPO in cyclohexane (undegassed), 1 ch(x) = 2.5 nm. To avoid energy transfer, both species were mixed electronically, by repetitive exchange of two cuvettes during the acquisition. Background was fixed to zero.

ered lifetimes and vibrational structures coincide with literature values.[7] Figure 2 (right) represents FAD as an example of a three-exponential decay. Note the IRF of 375 nm excitation in the fluorescence intensity contour map. Global analysis reveals three distinct lifetime components, whose individual values of single-channel analysis fall within the error given by global analysis (dashed lines). The deviations at the red side of the emission band are due to background contributions.

Photophysics of DAPI

Figure 3 displays three contour maps of an aging DAPI stock solution (methanol). The contribution of the slow, 2.4 ns component at the blue side of the emission band increases with the age of the stock solution and amounts to 7, 18, and 42%, respectively, of the total fluorescence intensity. Figure 3 (right) represents static emission spectra, monitoring the progress of decomposition at two temperatures and pH 5.3 in water. The dramatic increase in fluorescence intensity with time is accompanied by a blue-shift of the emission maximum. The insets show the corresponding first-order kinetic analyses of product formation at 40 and 75°C. The decomposition process at pH 3 is much slower, indicating that hydroxy-catalyzed hydrolysis[9] is the cause of the observed aging effect. It is recommended, therefore, to keep the stock of DAPI at pH 3 (H_2O/HCl) and 5°C. Glycine buffer should be avoided, since the amino acid tends to replace the NH_2 groups in DAPI, leading to spectroscopically similar products of probably deviant binding properties to DNA.

Figure 4 (top) shows the pH dependence of DAPI fluorescence dynamics. The short component of 135 $\pm$ 5 ps lifetime dominates the decay and is absolutely independent of pH for $1 < \text{pH} < 9$.[1] The long-lived component ($\tau = 1.8$–2.4 ns; weakly dependent on pH end λ_{ex})[1] at the blue side of the emission band is caused by decomposition products of DAPI (Fig. 3) and overlaps in emission wavelength and lifetime with the DAPI anion, whose contribution can be seen in the three-exponential analysis of the dynamics at pH 9.9. The fluorescence dynamics at higher pH values is more complex, due to the presence of two anionic species.[8]

Figure 4 (bottom) shows the analysis of the fluorescence dynamics of DAPI in methanol–water mixtures. The fluorescence dynamics in the various solvent mixtures are strictly one-exponential (disregarding the impurity contribution) and increase in lifetime with methanol content. We observe an excellent fit ($r = 0.995$) when plotting the corrected fluorescence lifetime against the polarity parameter, $E_T(30)$, strongly indicative of a polarity model of DAPI photophysics.

We did not observe any fluctuations of the DAPI fluorescence lifetime with pH for $1 < \text{pH} < 9$, lifetime distributions, deprotonation kinetics caused by water, or ground-state conformational equilibria.[11]

Kinetics of DAPI–DNA and DAPI–Cell Suspensions

Figure 5 (left) shows the contour map and three-exponential global analysis of a DAPI–DNA(λ) suspen-
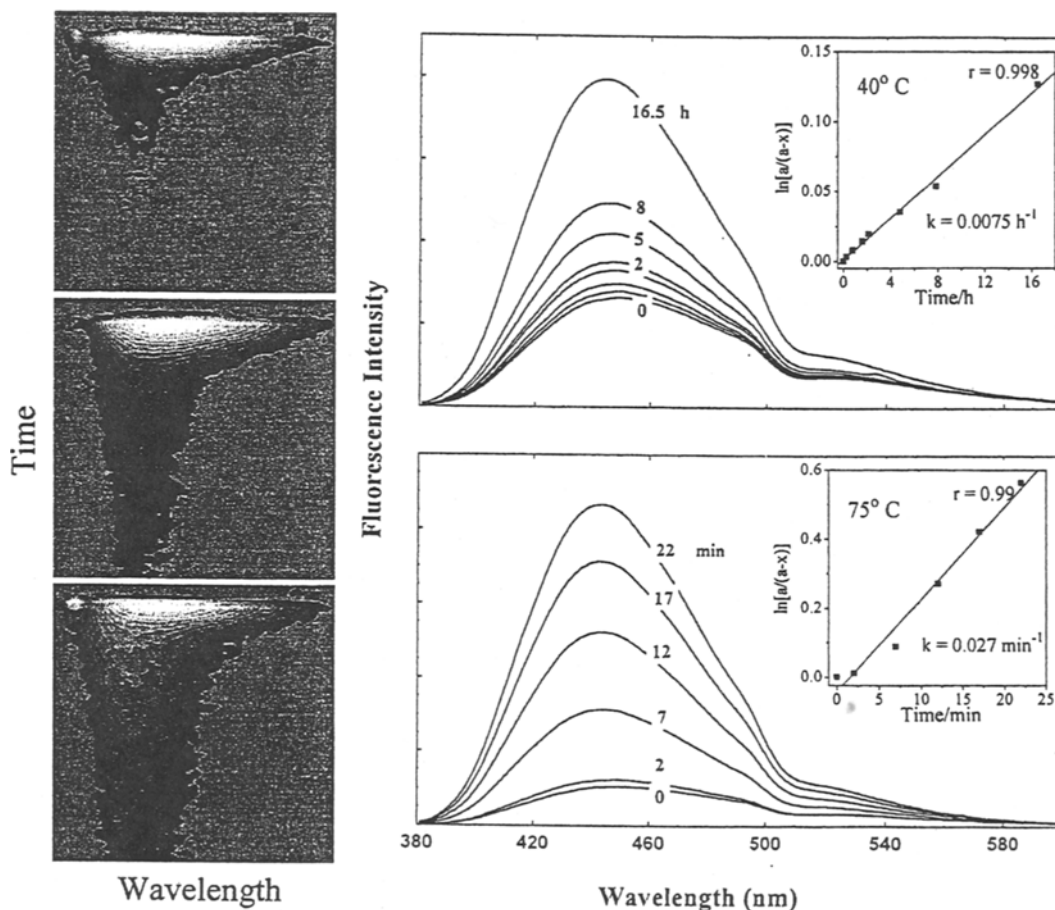
Fig. 3. Aging of DAPI stock solution. Left: Contour map of 1×10^{-5} M solution, prepared from fresh (top), 1-week-old (middle), and 5-week-old stock (bottom). Time axis (5 ns), top to bottom. The IRF of 375 nm excitation can be seen at top left. Right: Decomposition of DAPI at 40 and 75°C at pH 5.3. First-order kinetic analysis: the rate constants of product formation are 0.0075 h^{-1} and 0.027 min^{-1} at 40 and 75°C, respectively (insets). The analysis assumed same radiative lifetime for educt and product; $a = 1 \times 10^{-4}$ M DAPI stock, x = concentration of product.

sion. The short component, of 135 ps lifetime, is caused by free probe; the 1.1 ns component by bound DAPI; and the long-lived component, of 8.5 ns lifetime, at the red side of the emission band, by dimers or aggregates (see below). Four-exponential behavior was observed for DAPI–cell suspensions, with lifetimes of 140 ps, 0.9 ns, 2.5 ns, and 9 ns, accompanied by a red-shift of the individual emission maxima.

Models with one or two lifetime distributions (Gaussian or Lorentzian)[11] yielded fits always worse than that obtained by three- or four-exponential fitting.

DAPI–SDS Micelle System

Figure 5 (right) shows the static emission spectra of DAPI–SDS solutions. Initially, upon the addition of small quantities of SDS (1–5 µl), the emission is strongly quenched,[9] and the blue fluorescence turns yellow. At higher SDS concentrations (20–100 µl) the blue emission returns; the reversible color switch can be clearly seen by the unaided eye. This behavior is analogous to that observed for 3,3'-diethylthiacarbocyanine iodide[12a] and explained by dimer and aggregate formation of the dye in the premicellar region.[12b] At higher SDS concentrations micelles form and the aggregates are dissolved.

Cationic dyes reside on the negatively charged surface of SDS micelles. The polarity of the multi-anion surface had been determined to be $E_T(30) = 57.5$,[13] coincident with observed lifetimes of 1–3 ns in the micelle systems and the present polarity model in Fig. 5.
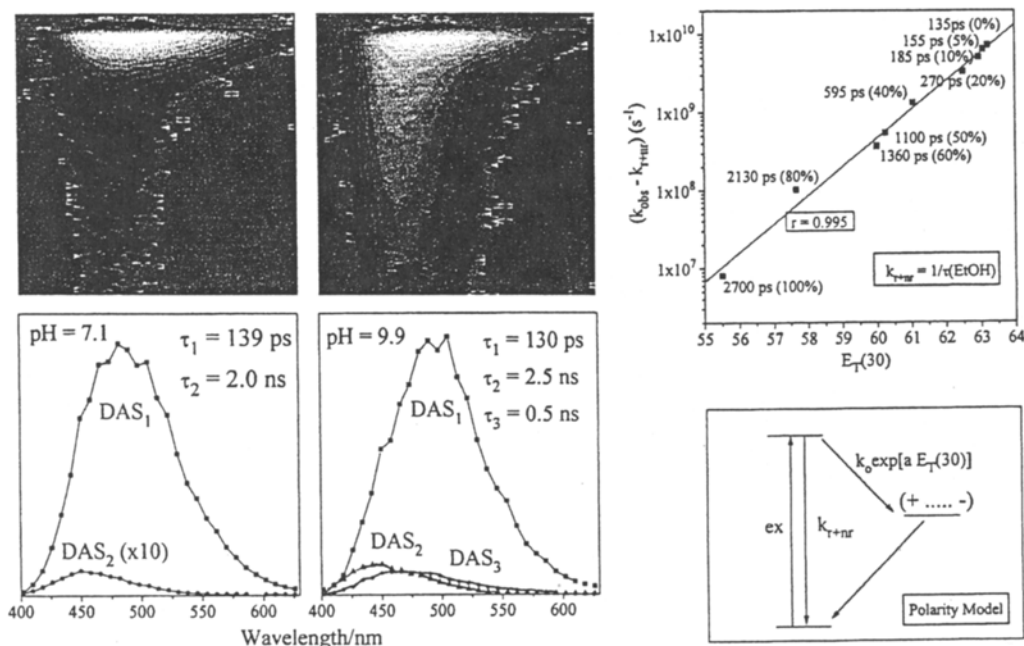
Fig. 4. Photophysics of DAPI. Left: pH dependence of 1×10^{-5} M DAPI at pH 7.1 and 9.9. The behavior at pH 7.1 is representative for the pH region $1 < pH < 9$. Right: Polarity model of DAPI photophysics. Top: Plot of corrected fluorescence lifetimes of DAPI in methanol–water mixtures vs $E_T(30)$ of the mixed solvents.[10] The observed lifetime of $\tau = 2.76$ ns in weakly polar ethanol was assumed to represent $k_r + k_{nr}$. Shown next to the data points are the observed lifetimes, with methanol concentrations in parentheses. Bottom: Polarity-dependent process, such as charge separation, dominating the excited-state kinetics.
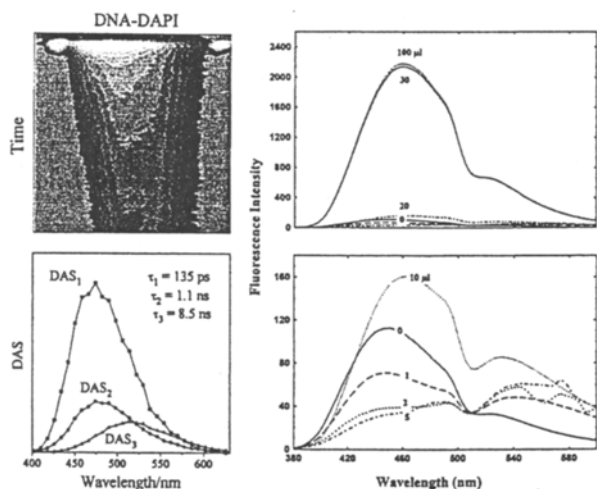

Fig. 5. DAPI–DNA(λ) and DAPI–SDS systems. Left: Contour map and three-exponential global analysis with DAS of the fluorescence kinetics of DNA–DAPI suspensions. $c(DAPI)/c(DNA) = 0.15$, $c(DAPI) = 3 \times 10^{-5}$ M, pH 8.1. Note the first (top left)- and second-order (top right) IRF in the contour map at 375 and 750 nm, respectively, used for calibration of the wavelength axis. Right: Static emission spectra of the DAPI–SDS system: successive addition (μl) of 0.04 M SDS stock solution to 2 ml of 3×10^{-6} M DAPI at pH 7.

Microscopic Imaging of C350–DNA and C350–Protein Complexes at Picosecond Time Resolution

Figure 6 (top) displays the image lines (schematic) seen by the DL detector of two test samples. Silk fibers and fungus tissue were stained by C350, excited at 514 nm, and observed through a 10 × objective at >600 nm. Figure 6 (middle) represents the corresponding contour maps and the results of global analysis. Both samples decay two-exponentially, with a common fast lifetime of 220 ps. The contribution of the slower component depends strongly on the spatial location in the case of the silk fiber sample (0.65 ns) but is independent (1.3 ns) within the fungus tissue. Figure 6 (bottom) shows time profiles, cut at the peak of a silk fiber (85% fast) and at the valley between two fibers (<5% fast). The rise of 140 ps, observed in the valleys, is attributed to multiscattered stray fluorescence and the associated decay time of 0.65 ns, therefore, is regarded as background.

From the above results, we conclude that the lifetime of the protein complex (silk) is 200 ps, whereas the DNA complex (fungus) shows a longer lifetime of 1.3 ns. Corroboration for this assignment was obtained by
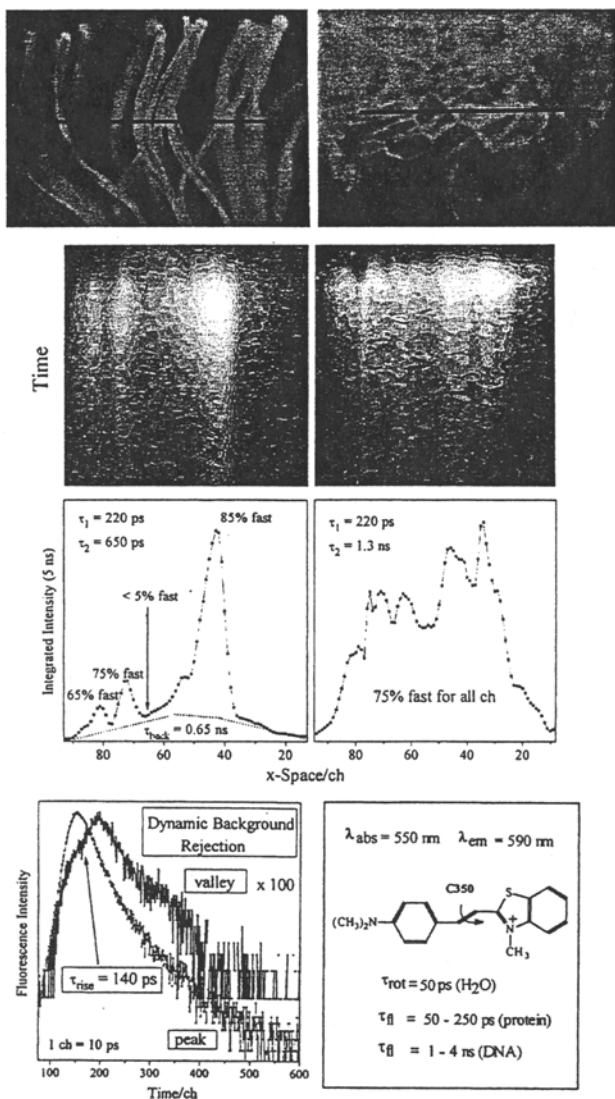
Fig. 6. Subnanosecond imaging. Top: Microscope images of silk fibers (left) and fungus tissue (right). Middle: Contour maps and global analysis of top. Bottom: Left—Dynamic background rejection. Two time profiles of middle left, cut at the peak of a fiber and at the valley between two fibers. Right—Structural formula of C350. The fluorescence lifetime in water is estimated to be 50 ps, originating in fast isomerization (arrow) in low-viscosity solvent, such as water.

the examination of protein–probe and DNA–probe suspensions, using C350 and TOTO as probe molecules. We observed short lifetimes of 50 ps (C350) and 150 ps (TOTO) in the case of protein (albumin), whereas DNA (herring sperm) displayed much longer lifetimes of 1.6–3.4 ns (two-exponential, C350) and 0.4–4.6 ns (three-exponential, TOTO).

SUMMARY

Picosecond time resolution is indispensable for dynamic stray-light rejection and kinetic discrimination of probe–protein and probe–DNA complexes. Since most molecular probes do not probe an individual physical property exclusively—EB, for instance—has a considerable sensitivity for polarity and does not only indicate the presence of water,[14] we are currently developing a complementary multiprobe approach, utilizing kinetic information on the picosecond time scale of probe complexes together with improved understanding of underlying probe photophysics.

ACKNOWLEDGMENTS

REFERENCES

1a. K. Kemnitz, L. Pfeifer, R. Paul, F. Fink, and A. Bergmann (1995) *Proc. SPIE* **2628**, 2.
1b. K. Kemnitz, R. Paul, J. Coppey, and M. Coppey-Moisan (1996) *Proc. SPIE*, **2926**, 177.
1c. K. Kemnitz, L. Pfeifer, M. R. Ainbund (1997) *Nucl. Instr. and Meth., Sec. A*, in press.
2. D. V. O'Connor and D. Phillips (1984) *Time-Correlated Single Photon Counting*, Academic Press, New York.
3. (a) M. R. Ainbund, O. E. Buevich, V. F. Kamalov, G. A. Menshikov, and B. N. Toleutaev (1992) *Rev. Sci. Instr.* **63**, 3274. (b) U.S. patent No. 5,148,031.
4. M. Lampton and R. F. Malina (1976) *Rev. Sci. Instr.* **47**, 1360.
5. A. A. Samarsky, I. D. Rodionov, M. Yu. Knizhnikov, and A. N. Ponomarev (1992) *Proc. SPIE* **2107**, 476.
6. M. R. Ainbund, S. Yu. Arzhantsev, A. Yu. Chikishev, N. I. Koroteev, A. P. Shkurinov, B. N. Toleutaev, E. V. Turbin, A. Lehmann, L. Pfeifer, F. Fink, and K. Kemnitz (1997) 2nd Conference on Fluorescence Microscopy and Fluorescent Probes, Prague, Plenum Press.
7. (a) J. R. Lakowicz, H. Szmacinski, K. Nowaczyk, and M. L. Johnson (1992) *Proc. Natl. Acad. Sci. USA* **89**, 1271. (b) R. A. Lampert, L. A. Chewter, D. Phillips, D. V. O'Connor, A. J. Roberts, and S. R. Meech (1983) *Anal. Chem.* **55**, 68.
8. K. Kemnitz, L. Pfeifer, and M. Coppey-Moisan, in preparation.
9. J. Kapuscinski and B. Skoczylas (1978) *Nucl. Acid Res.* **5**, 3775.
10. $E_T(30)$ values extrapolated according to procedure, described by K. G. Casey and E. L. Quitevis (1988) *J. Phys. Chem.* **92**, 6590.
11. (a) M. L. Barcellona and E. Gratton (1989) *Biochim. Biophys. Acta* **993**, 174. (b) M. L. Barcellona, G. Cardiel, and E. Gratton (1990) *Biochem. Biophys. Res. Comm.* **170**, 270. (c) M. L. Barcellona and E. Gratton (1991) *Biophys. Chem.* **40**, 223.
12. (a) H. Sato, M. Kawasaki, K. Kasatani, Y. Kusumoto, N. Nakashima, and K. Yoshihara (1980) *Chem. Lett.* 1529. (b) P. Mukerjee and K. J. Mysels (1955) *J. Am. Chem. Soc.* **77**, 2937.
13. K. A. Zachariasse, N. Van Phuc, and B. Kozankiewicz (1981) *J. Phys. Chem.* **85**, 2676.
14. K. Kemnitz, et al. in preparation.